Visualizing Higher-Fold Topology in Chiral Crystals

Tyler A. Cochran,[1] Ilya Belopolski,[1] Kaustuv Manna,[2,3] Mohammad Yahyavi,[4,5] Yiyuan Liu,[6] Daniel S. Sanchez,[1] Zi-Jia Cheng,[1] Xian P. Yang,[1] Daniel Multer,[1] Jia-Xin Yin,[1] Horst Borrmann,[2] Alla Chikina,[7] Jonas A. Krieger,[7,8] Jaime Sánchez-Barriga,[9,10] Patrick Le Fèvre,[11] François Bertran,[1] Vladimir N. Strocov,[7] Jonathan D. Denlinger,[12] Tay-Rong Chang,[4] Shuang Jia,[5] Claudia Felser,[2] Hsin Lin,[13] Guoqing Chang,[5,†] and M. Zahid Hasan[1,14,15,*]

[1]*Laboratory for Topological Quantum Matter and Advanced Spectroscopy (B7), Department of Physics, Princeton University, Princeton, New Jersey 08544, USA*
[2]*Max Planck Institute for Chemical Physics of Solids, 01187 Dresden, Germany*
[3]*Department of Physics, Indian Institute of Technology Delhi, Hauz Khas, New Delhi 110016, India*
[4]*Department of Physics, National Cheng Kung University, Tainan 70101, Taiwan*
[5]*Division of Physics and Applied Physics, School of Physical and Mathematical Sciences, Nanyang Technological University, 21 Nanyang Link 637371, Singapore*
[6]*International Center for Quantum Materials, School of Physics, Peking University, Beijing 100871, China*
[7]*Swiss Light Source, Paul Scherrer Institute, 5232 Villigen, Switzerland*
[8]*Laboratory for Muon Spin Spectroscopy, Paul Scherrer Institute, 5232 Villigen, Switzerland*
[9]*Helmholtz-Zentrum Berlin für Materialien und Energie, Elektronenspeicherring BESSY II, Albert-Einstein Strasse 15, 12489 Berlin, Germany*
[10]*IMDEA Nanoscience, C/ Faraday 9, Campus de Cantoblanco, 28049 Madrid, Spain*
[11]*SOLEIL Synchrotron, L'Orme des Merisiers, Départementale 128, F-91190 Saint-Aubin, France*
[12]*Advanced Light Source, Lawrence Berkeley National Laboratory, Berkeley, California 94720, USA*
[13]*Institute of Physics, Academia Sinica, Taipei 11529, Taiwan*
[14]*Princeton Institute for Science and Technology of Materials, Princeton University, Princeton, New Jersey 08544, USA*
[15]*Lawrence Berkeley National Laboratory, Berkeley, California 94720, USA*

(Received 19 October 2021; revised 18 January 2022; accepted 14 December 2022; published 8 February 2023)

Novel topological phases of matter are fruitful platforms for the discovery of unconventional electromagnetic phenomena. Higher-fold topology is one example, where the low-energy description goes beyond standard model analogs. Despite intensive experimental studies, conclusive evidence remains elusive for the *multigap topological nature of higher-fold chiral fermions*. In this Letter, we leverage a combination of fine-tuned chemical engineering and photoemission spectroscopy with photon energy contrast to discover the higher-fold topology of a chiral crystal. We identify all bulk branches of a higher-fold chiral fermion for the first time, critically important for allowing us to explore unique Fermi arc surface states in multiple interband gaps, which exhibit an emergent ladder structure. Through designer chemical gating of the samples in combination with our measurements, we uncover an unprecedented multigap bulk boundary correspondence. Our demonstration of multigap electronic topology will propel future research on unconventional topological responses.

DOI: 10.1103/PhysRevLett.130.066402

Traditional topological quantum states have often been characterized by a single Chern number, such as the chiral charge of a Weyl fermion or the quantum anomalous Hall (QAH) conductance of a two-dimensional insulator [1–6]. The observation and manipulation of multi-Chern number topological structures promise to open new opportunities for fundamental physics and applications [7,8]. Already, sequences of Chern insulating states have been observed in magic-angle twisted bilayer graphene [9–15], while large Chern numbers were engineered by the assembly of multiple QAH layers [2,16]. In both cases the effects arise only at ~ 10 meV energy scales and ~ 200 mK temperatures, limiting the ability for spectroscopic study and technological application. However, multi-Chern number states are also associated with higher-fold chiral fermions in three-dimensional bulk topological semimetals, which can naturally possess a 1 eV energy scale at room temperature [6]. This prospect, if achieved, will allow for the study of generalizations of the quantized circular photogalvanic effect [17–20], exotic multi-Fermi arc nonlinear optical effects [21,22], and multi-Fermi arc quantum oscillations [23]. However, despite this promising outlook, the multi-Chern nature of higher-fold chiral fermions has proven challenging to observe, despite considerable effort on stoichiometric B20 compounds [24–27]. Therefore, an urgent experimental challenge is to obtain a degree of

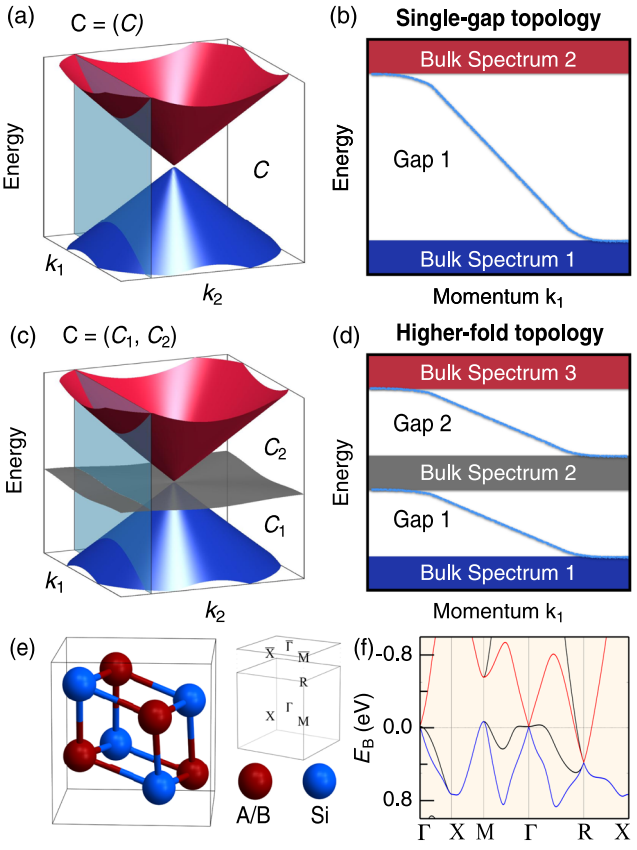

FIG. 1. Higher-fold topology beyond Weyl and Dirac. (a) Schematic of a two-band system corresponding to a Weyl fermion in three dimensions. (b) Schematic of bulk-boundary correspondence of a one-gap system with a boundary chiral mode. The momentum path corresponds to the blue plane in Fig. 1(a). (c) Schematic of a chiral fermion with three bulk branches and two topologically nontrivial energy gaps. (d) Schematic of bulk-boundary correspondence of a two-gap system with boundary chiral modes. The momentum path corresponds to the blue plane in Fig. 1(c). (e) Crystal structure of the $A_{1-x}B_x$Si substitutional alloy in the $P2_13$ space group (#198), with A = Rh and B = Ni. The bulk and (001) surface Brillouin zone. (f) *Ab initio* band structure calculation along high-symmetry lines of RhSi.

tunability in these materials in order to understand their unconventional topological nature.

Higher-fold chiral fermions can be understood as a generalization of more familiar Weyl fermions, being themselves twofold chiral fermions. For Weyl fermions, one topological invariant is defined within the band gap on k-space manifolds enclosing a twofold degeneracy, the chiral charge C [Fig. 1(a)]. As a consequence, one set of boundary states is topologically protected within the gap [Fig. 1(b)]. By extending this paradigm to higher-fold fermions, the set of possibilities becomes more diverse. Dirac-like nonchiral fermions have a chiral charge of zero in each gap [28–32], whereas Weyl-like chiral fermions have nonzero chiral charge in multiple gaps [18,33–36]. For an N-fold chiral fermion, we introduce the multigap chiral charge $\mathbf{C} = (C_1, C_2, \ldots, C_{N-1})$, which includes one integer for each band gap [Fig. 1(c)]. From here, the bulk-boundary correspondence specifies that in gap i there are C_i chiral surface states (Fermi arcs). These states are also called chiral because of the presence of a net nonzero number of left or right moving quasiparticles for a chosen chemical potential along a closed path in the surface Brillouin zone. In the multigap case, there are a net nonzero number of left or right movers in multiple gaps, leading to chiral Fermi arcs that are stacked in the energy direction [Fig. 1(d)]. Therefore, to discover an N-fold chiral fermion with higher-fold topology, one needs to directly observe all the bulk branches [Fig. 1(c)], and use the Fermi arcs on the surface to determine the multigap chiral charge [Fig. 1(d)].

In order to establish the topological nature of any band structure, the bulk-boundary correspondence must be rigorously established experimentally [37–39]. In the case of higher-fold chiral fermions, the two key experimental signatures are (1) resolving all the bulk bands that become degenerate at a higher-fold chiral fermion, and (2) showing a nontrivial Chern number in each interband gap. Verifying these criteria amounts to confirming the multigap bulk boundary correspondence. In higher-fold topological material candidates to date, giant Fermi arc states and linear dispersions have been observed, indicating the presence of Weyl-like quasiparticles [24–27]. However, neither criterion for higher-fold topology listed above has been met by any experiment, on any material (see Sec. I. A. of the Supplemental Material [40]).

In the search for an ideal material candidate to study higher-fold topology, we consider crystals in structurally chiral space group $P2_13$ (#198), where nonzero Chern numbers and bulk conelike dispersions have recently been observed [24–27]. Materials in this space group are promising because conical bands are predicted to arise from a threefold chiral fermion at the Γ point, naturally providing a platform for multiple topological band gaps [Figs. 1(e), 1(f), and 1(g)] [33,34].

In this Letter, we chemically engineer the substitutional alloy $Rh_{1-x}Ni_xSi$, to realize tunable chemical gating (See Secs. I. B., I. C., and II. A. of the Supplemental Material [40] and Refs. [41–43,56]). Rigorous Laue, as well as single crystal, X-ray diffraction measurements show that our sample exhibits excellent crystal quality, and possesses the desired structurally chiral space group $P2_13$ (#198). Detailed chemical analysis indicates that our $Rh_{1-x}Ni_xSi$ sample possesses $x = 0.05$. The Flack parameter was refined to $-0.01(11)$ throughout the sample, indicating that only one structurally chiral domain is present. Importantly, the presence of Ni does not induce any magnetism as the sample was found to be diamagnetic down to 10 K.

Using bulk-sensitive soft x-ray angle-resolved photoemission spectroscopy (SXARPES), we first search for higher-fold degeneracies using 550 eV incident photons (see Sec. II. B. of the Supplemental Material [40] and

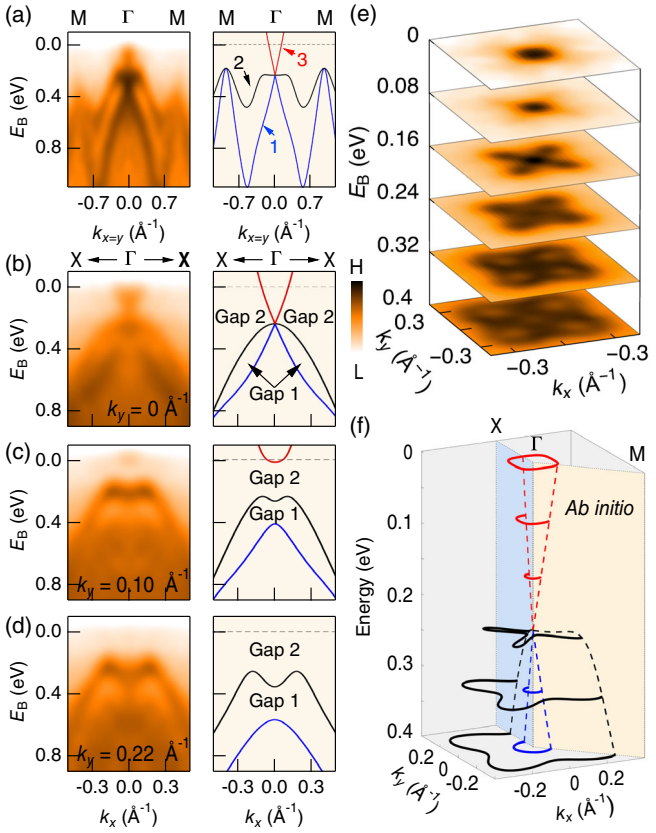

FIG. 2. Topological chiral fermion at the Γ point. (a) Bulk sensitive SXARPES measured using 550 eV incident photons and *ab initio* E_B vs k spectrum along the M-Γ-M line, showing three bands becoming degenerate at the Γ point. (b) SXARPES and *ab initio* spectra along the X-Γ-X line, confirming three bands dispersing away from the degeneracy point. (c) SXARPES E_B vs k spectrum and *ab initio* calculation along a path shifted to $k_y = 0.1$ Å^{-1}. Along this momentum path, gap 1 and gap 2 can be identified. (d) SXARPES spectrum and *ab initio* calculation along a path further shifted to $k_y = 0.22$ Å^{-1}. (e) SXARPES measured stack of constant E_B contours at the Γ point, showing the band structure evolution through the degeneracy point. (f) *Ab initio* calculation of constant E_B stack.

Refs. [44–46,57]). We find that for the M-Γ-M binding energy vs crystal momentum (E_B vs k) dispersion, three bands become degenerate 240 meV below the Fermi level at the Γ point, which is also reflected in the *ab initio* calculation [Fig. 2(a)]. Away from the Γ point the energy separation between all three bands becomes clear; we define gaps 1 and 2 to be the separations between bands 1, 2, and 3 away from the Γ point. To further verify our finding of a threefold degeneracy, we measure the E_B vs k dispersion along another path, X-Γ-X [Fig. 2(b)]. Here we also observe a threefold degeneracy at the Γ point. Along this new path, gap 1 is diminished compared with M-Γ-M. We confirm our results by systematically examining E_B vs k dispersions slightly away from the Γ point. As the X-Γ-X dispersion is shifted in the k_y direction, band 3 quickly retreats above the Fermi level, while band 2 disperses very little, and band 1 falls to deeper binding energies [Figs. 2(c) and 2(d)]. Our experimental results confirm the bulk dispersion of a threefold chiral fermion: a linear crossing between bands 1 and 3 is degenerate with a nearly flat band 2 at the Γ point. These three bands naturally give rise to two gaps in which the topological surface states should reside.

To gain additional insight into the threefold chiral fermion, we examine constant E_B contours. At $E_B = 400$ meV, below the degeneracy point, two bands are observed [Figs. 2(e) and 2(f)]. Band 1 is circular, whereas band 2 has an apparent distortion, which explains the variation between the band separations along the $\Gamma - X$ and $\Gamma - M$ directions. Above the degeneracy point at the Fermi level, only one band is observed; it is circular. Therefore, bands 1 and 3 form a nearly isotropic cone, whereas band 2 has a paraboliclike dispersion that is distorted by the cubic crystal symmetry. These results allow us to conclude we have observed all three branches of a threefold chiral fermion at the Γ point.

Having characterized the threefold bulk crossing, we now present experimental evidence of its nontrivial higher-fold topology. Using surface-sensitive ultraviolet angle-resolve photoemission spectroscopy (UVARPES), we directly observe topological surface states in two gapped regions of the bulk electronic structure. By utilizing 85 eV incident photons, the measured (001) Fermi surface covers multiple surface Brillouin zones [Fig. 3(a)]. Long states are observed stretching across each Brillouin zone from the $\bar{\Gamma}$ point to the $\bar{M}$ point. Further decreasing the photon energy to 40 eV to improve energy and momentum resolution, these states disperse along the same trajectory. Focusing near the $\bar{\Gamma}$ point, we observe the surface states have a high photoemission intensity [Fig. 3(b)]. By taking the second derivative of the spectrum, we see the states are discontinuous at the $\bar{\Gamma}$ point [Fig. 3(c)]. To explain this, we turn to the bulk spectrum [Fig. 3(d)]. Overlaying the surface onto the bulk dispersion, it is evident that the surface states emanate from the bulk bands as stipulated by the bulk-boundary correspondence for Fermi arcs [Fig. 3(e)]. Further understanding of these states can be gained by analyzing their E_B vs k dispersion near the $\bar{\Gamma}$ point. At negative k_y, one isolated right-moving chiral mode is observed, which corresponds to a Chern number of $C(k_y < 0) = 1$ along the bulk plane that projects onto the line $k_y = -0.33$ Å^{-1} [Fig. 3(f)]. At $k_y = 0$ Å^{-1}, the chiral state and its time-reversal partner connect directly to the projection of the bulk degeneracy point, showing the surface to bulk connectivity [Fig. 3(g)]. Moving to positive k_y, one isolated left-moving chiral mode is observed, indicating $C(k_y > 0) = -1$ on the corresponding bulk plane [Fig. 3(h)]. Together, these three dispersions provide strong evidence that the surface states are topological Fermi arcs, connecting bands 2 and 3 of the bulk threefold chiral fermion. Moreover, these measurements reveal the detailed nature of Fermi arc switching at a higher-fold fermion. We

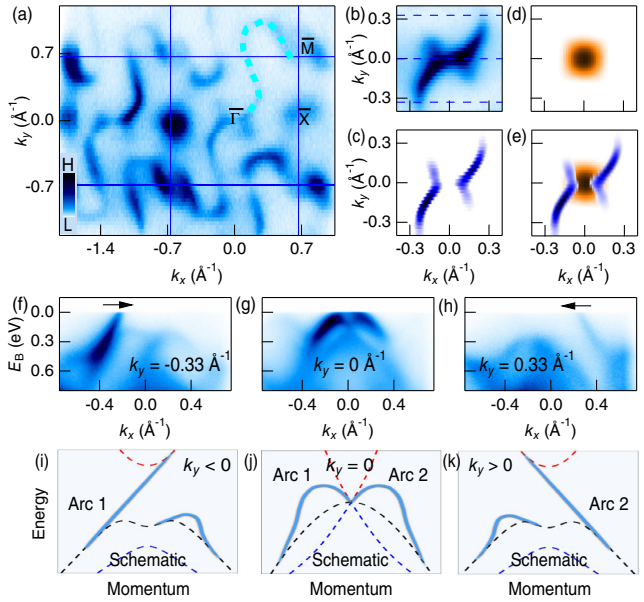

FIG. 3. Fermi arc switching in momentum space. (a) Surface sensitive UVARPES measured Fermi surface from (001) surface, utiliizing 85 eV incident photons. Long Fermi arc surface states connect pockets at $\bar{\Gamma}$ and $\bar{\mathrm{M}}$ as indicated by the dashed cyan line. (b) UVARPES measured Fermi surface at the $\bar{\Gamma}$ point with 40 eV incident photons. (c) Second derivative of spectrum in Fig. 3(b). (d) SXARPES measured Fermi surface at the Γ point. (e) Overlay of Fig. 3(c) on Fig. 3(d) showing the Fermi arcs connecting to the bulk band. (f)–(h) E_B vs k UVARPES spectra showing chiral Fermi arc surface states along paths defined by the dotted lines in Fig. 3(b). Arrows indicate chiral modes at the Fermi level, which switch at the threefold chiral fermion at the $\bar{\Gamma}$ point. (i)–(k) Schematics of chiral Fermi arcs (solid blue lines) and bulk bands (dotted lines) depicting the Fermi arc switching at the $\bar{\Gamma}$ point.

clearly see a surface state transition from topological (connecting bands 2 and 3) to trivial (starting and ending at band 2) as the E_B vs k dispersion is scanned across the degeneracy point, as illustrated in the schematics [Figs. 3(i), 3(j), and 3(k)]. To extract the chiral charge for gap 2, we note that the difference between the Chern numbers along two lines is equal to the chiral charge enclosed by those lines [47]. In this case, we obtain that the chiral charge in gap 2 is $C_2 = C(k_y < 0) - C(k_y > 0) = 1 - (-1) = 2$.

To determine the topology of gap 1, we examine the band structure below the Fermi level. A constant E_B contour measured at $E_B = 300$ meV shows signatures of multiple chiral modes indicated by dashed cyan lines [Fig. 4(a)]. While the Fermi arcs in gap 2 are still present near the edge of Fig. 4(a), there is another set of states residing closer to $\bar{\Gamma}$. To better resolve these states, we take the second derivative of the constant E_B spectrum [Fig. 4(b)], and observe that the inner states are disconnected and distinct from the outer Fermi arcs. To know which gap to associate these surface states with, we contrast the UVARPES and the bulk SXARPES spectra [Fig. 4(c)]. By comparing the surface states and bulk constant E_B contours [Fig. 4(d)], we see that the inner surface states propagate from band 1 to band 2, consistent with these states being topological Fermi arcs in gap 1 [Fig. 4(e)]. To confirm this, we measure E_B vs k UVARPES spectra along the path indicated by the dashed, dark blue line in Fig. 4(a). We identify two distinct chiral modes [Fig. 4(f)]. Overlaying the second derivative of the surface state spectrum [Fig. 4(g)] onto the bulk spectrum [Fig. 4(g)], we see that one chiral mode lies entirely within gap 1, while the other disperses in gap 2, forming a ladder structure [Fig. 4(i)]. The state in gap 2 is the Fermi arc already discussed in Fig. 3. The chiral state in gap 1 is a second Fermi arc, connecting bands 1 and 2. With an identical procedure to that carried out for gap 2, the chiral charge of gap 1 can be experimentally assigned to be $C_1 = 2$. Together our measurements in gap 1 and 2 visualize a Fermi arc ladder, which demonstrates the multigap bulk boundary correspondence for a higher-fold chiral fermion with multigap chiral charge $\mathbf{C} = (2, 2)$ [Fig. 4(j)].

Through the multigap bulk-boundary correspondence, we have discovered higher-fold topology in a threefold chiral fermion, with multigap chiral charge $\mathbf{C} = (2, 2)$. This work further motivates transport and optical research on higher-fold topological materials. Indeed, our material-realistic theoretical simulations presented in the Supplemental Material [40] reveal a giant enhancement to optical sum frequency response, unique to crystals with multiple topological interband gaps (see Secs. I. D. and II. C. of the Supplemental Material [40] and Refs. [48–50,58,59]). This stems from optical resonances across multiple topological gaps, which is only possible in the multigap regime. Furthermore, by considering our chemical engineering in the simulations we elucidate the possibility of unprecedented photocurrent response of our samples. Our technique of freely doping the Fermi level and preserving the topological bands provides a concrete pathway to realize a tunable quantized circular photogalvanic effect, which has been elusive in pristine RhSi and CoSi samples (see Sec. I. E. of the Supplemental Material [40] and Refs. [51,52]). Specifically, we predict quantized photocurrent behavior not only in our $Rh_{1-x}Ni_xSi$ samples, but also in $Rh_{1-x}Fe_xSi$. These results underscore the importance of the present study, while motivating further transport and optical research on higher-fold topological materials. For example, we expect exotic behavior when considering interarc and arc-to-bulk and bulk-to-arc transitions in RhSi, inducing unconventional surface photocurrents with applications to thin film devices [21]. Furthermore, the multigap topology presented here is not restricted to electronic crystals, and can be realized in mechanical [53], phononic [60], photonic [54], cold atom [55], qubit [61], and even atmospheric systems [62], opening up opportunities for future research.

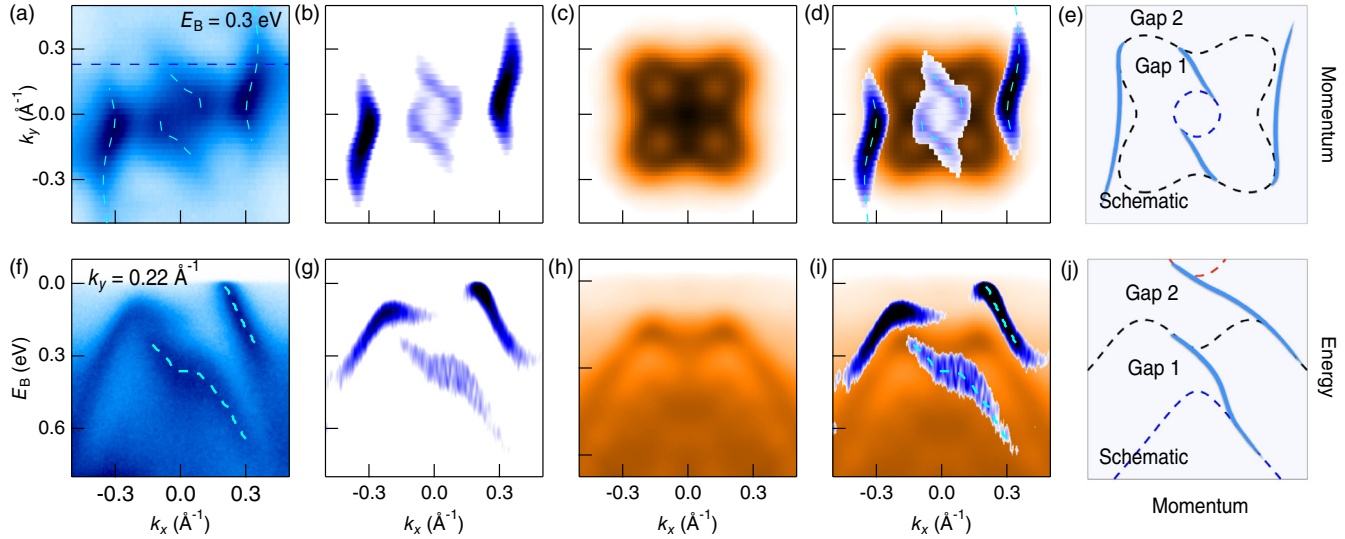

FIG. 4. Multigap chiral charge and a Fermi arc ladder. (a) and (b) UVARPES measured constant E_B contour at $E_B = 300$ meV [Fig. 4(a)] and second-derivative [Fig. 4(b)] at the $\bar{\Gamma}$ point. Both inner and outer states are indicated by cyan dashed lines in Fig. 4(a). (c) SXARPES constant E_B contour at $E_B = 300$ meV at the Γ point. (d) Overlay of Fig. 4(b) onto Fig. 4(c); the inner surface states lie within the bulk projection of band 2. (e) Schematic constant E_B contour showing chiral states (thick blue lines) in gap 1 and gap 2 of the bulk threefold chiral fermion (dotted lines). (f) and (g) UVARPES measured E_B vs k cut at $k_y = 0.22$ Å^{-1} [Fig. 4(f)] and second derivative [Fig. 4(g)], along the path indicated by the dark blue dashed line in Fig. 4(a). Two disconnected chiral modes are observed (dashed cyan lines). (h) SXARPES measured spectrum along the same path as Fig. 4(f) at $k_y = 0.22$ Å^{-1}. (i) Overlay of Fig. 4(g) onto Fig. 4(h), showing topological surface states propagating in gap 1 and 2 respectively. (j) Schematic E_B vs k plot showing the Fermi arc ladder (thick blue lines).

The authors acknowledge Songtian S. Zhang and Nana Shumiya for useful conversations during manuscript preparations. The authors also acknowledge Takayuki Muro for beamline support at SPring-8 BL25SU. Work at Princeton University and Princeton-led synchrotron based ARPES measurements were supported by the United States Department of Energy (US DOE) under the Basic Energy Sciences program (Grant No. DOE/BES DE-FG-02-05ER46200). This research used resources of the Advanced Light Source, which is a DOE Office of Science User Facility under Contract No. DE-AC02-05CH11231. Synchrotron radiation experiments were performed at the BL25SU of SPring-8 with the approval of the Japan Synchrotron Radiation Research Institute (JASRI) (Proposal No. 2018A1684 and No. 2019A1696). We acknowledge the Paul Scherrer Institut, Villigen, Switzerland, for provision of synchrotron radiation beamtime at the ADRESS beamline of the Swiss Light Source. We acknowledge SOLEIL for provision of synchrotron radiation facilities at the CASSIOPÉE beamline. Additional ARPES measurements were performed at the RGBL-2 end station at the U125/2 undulator beamline of BESSY II. T. A. C. was supported by the National Science Foundation Graduate Research Fellowship Program under Grant No. DGE-1656466. J. S.-B. gratefully acknowledges financial support from the Impuls-und Vernetzungsfonds der Helmholtz-Gemeinschaft under Grant No. HRSF-0067. K. M. and C. F. thank the European Research Council (ERC) for financial support with Advanced Grant No. (742068) "TOP-MAT". J. A. K. acknowledges support from the Swiss National Science Foundation (SNF-Grant No. 200021_165910). The work at Nanyang Technological University is supported by the National Research Foundation, Singapore, under its NRF Fellowship Award (NRF-NRFF13-2021-0010) and the Nanyang Assistant Professorship grant from Nanyang Technological University. K. M. acknowledges the Department of Atomic Energy (DAE), Government of India, for the funding support via the Young Scientist's Research Award (YSRA) via Grant No. 58/20/03/2021-BRNS/37084 and the Max Planck Society for the funding support under the Max Planck–India partner group project.

T. A. C., I. B., and G. C. contributed equally to this work.

*Corresponding author.
mzhasan@princeton.edu
†Corresponding author.
guoqing.chang@ntu.edu.sg

[1] K. He, Y. Wang, and Q.-K. Xue, Annu. Rev. Condens. Matter Phys. **9**, 329 (2018).
[2] Y. Tokura, K. Yasuda, and A. Tsukazaki, Nat. Rev. Phys. **1**, 126 (2019).

[3] N. P. Armitage, E. J. Mele, and A. Vishwanath, Rev. Mod. Phys. **90**, 015001 (2018).
[4] B. Yan and C. Felser, Annu. Rev. Condens. Matter Phys. **8**, 337 (2017).
[5] A. Burkov, Annu. Rev. Condens. Matter Phys. **9**, 359 (2018).
[6] M. Z. Hasan, G. Chang, I. Belopolski, G. Bian, S.-Y. Xu, and J.-X. Yin, Nat. Rev. Mater. **6**, 784 (2021).
[7] Y. Tokura, M. Kawasaki, and N. Nagaosa, Nat. Phys. **13**, 1056 (2017).
[8] D. N. Basov, R. D. Averitt, and D. Hsieh, Nat. Mater. **16**, 1077 (2017).
[9] K. P. Nuckolls, M. Oh, D. Wong, B. Lian, K. Watanabe, T. Taniguchi, B. A. Bernevig, and A. Yazdani, Nature (London) **588**, 610 (2020).
[10] Y. Saito, J. Ge, L. Rademaker, K. Watanabe, T. Taniguchi, D. A. Abanin, and A. F. Young, Nat. Phys. **17**, 478 (2021).
[11] Y. Choi, H. Kim, Y. Peng, A. Thomson, C. Lewandowski, R. Polski, Y. Zhang, H. S. Arora, K. Watanabe, T. Taniguchi, J. Alicea, and S. Nadj-Perge, Nature (London) **589**, 536 (2021).
[12] S. Wu, Z. Zhang, K. Watanabe, T. Taniguchi, and E. Y. Andrei, Nat. Mater. **20**, 488 (2021).
[13] I. Das, X. Lu, J. Herzog-Arbeitman, Z.-D. Song, K. Watanabe, T. Taniguchi, B. A. Bernevig, and D. K. Efetov, Nat. Phys. **17**, 710 (2021).
[14] J. M. Park, Y. Cao, K. Watanabe, T. Taniguchi, and P. Jarillo-Herrero, Nature (London) **592**, 43 (2021).
[15] A. T. Pierce, Y. Xie, J. M. Park, E. Khalaf, S. H. Lee, Y. Cao, D. E. Parker, P. R. Forrester, S. Chen, K. Watanabe, T. Taniguchi, A. Vishwanath, P. Jarillo-Herrero, and A. Yacoby, Nat. Phys. **17**, 1210 (2021).
[16] Y.-F. Zhao, R. Zhang, R. Mei, L.-J. Zhou, H. Yi, Y.-Q. Zhang, J. Yu, R. Xiao, K. Wang, N. Samarth, M. H. W. Chan, C.-X. Liu, and C.-Z. Chang, Nature (London) **588**, 419 (2020).
[17] F. de Juan, A. G. Grushin, T. Morimoto, and J. E. Moore, Nat. Commun. **8**, 15995 (2017).
[18] G. Chang, B. J. Wieder, F. Schindler, D. S. Sanchez, I. Belopolski, S.-M. Huang, B. Singh, D. Wu, T.-R. Chang, T. Neupert, S.-Y. Xu, H. Lin, and M. Z. Hasan, Nat. Mater. **17**, 978 (2018).
[19] D. Rees, K. Manna, B. Lu, T. Morimoto, H. Borrmann, C. Felser, J. E. Moore, D. H. Torchinsky, and J. Orenstein, Sci. Adv. **6**, eaba0509 (2020).
[20] B. Xu, Z. Fang, M.-Á. Sánchez-Martínez, J. W. F. Venderbos, Z. Ni, T. Qiu, K. Manna, K. Wang, J. Paglione, C. Bernhard, C. Felser, E. J. Mele, A. G. Grushin, A. M. Rappe, and L. Wu, Proc. Natl. Acad. Sci. U.S.A. **117**, 27104 (2020).
[21] G. Chang, J.-X. Yin, T. Neupert, D. S. Sanchez, I. Belopolski, S. S. Zhang, T. A. Cochran, Z.-J. Cheng, M.-C. Hsu, S.-M. Huang, B. Lian, S.-Y. Xu, H. Lin, and M. Z. Hasan, Phys. Rev. Lett. **124**, 166404 (2020).
[22] D. Rees, B. Lu, Y. Sun, K. Manna, R. Özgür, S. Subedi, H. Borrmann, C. Felser, J. Orenstein, and D. H. Torchinsky, Phys. Rev. Lett. **127**, 157405 (2021).
[23] P. J. W. Moll, N. L. Nair, T. Helm, A. C. Potter, I. Kimchi, A. Vishwanath, and J. G. Analytis, Nature (London) **535**, 266 (2016).
[24] D. S. Sanchez *et al.*, Nature (London) **567**, 500 (2019).
[25] Z. Rao, H. Li, T. Zhang, S. Tian, C. Li, B. Fu, C. Tang, L. Wang, Z. Li, W. Fan, J. Li, Y. Huang, Z. Liu, Y. Long, C. Fang, H. Weng, Y. Shi, H. Lei, Y. Sun, T. Qian, and H. Ding, Nature (London) **567**, 496 (2019).
[26] N. B. M. Schröter, D. Pei, M. G. Vergniory, Y. Sun, K. Manna, F. de Juan, J. A. Krieger, V. Süss, M. Schmidt, P. Dudin, B. Bradlyn, T. K. Kim, T. Schmitt, C. Cacho, C. Felser, V. N. Strocov, and Y. Chen, Nat. Phys. **15**, 759 (2019).
[27] D. Takane, Z. Wang, S. Souma, K. Nakayama, T. Nakamura, H. Oinuma, Y. Nakata, H. Iwasawa, C. Cacho, T. Kim, K. Horiba, H. Kumigashira, T. Takahashi, Y. Ando, and T. Sato, Phys. Rev. Lett. **122**, 076402 (2019).
[28] B. J. Wieder, Y. Kim, A. M. Rappe, and C. L. Kane, Phys. Rev. Lett. **116**, 186402 (2016).
[29] G. Chang, S.-Y. Xu, S.-M. Huang, D. S. Sanchez, C.-H. Hsu, G. Bian, Z.-M. Yu, I. Belopolski, N. Alidoust, H. Zheng, T.-R. Chang, H.-T. Jeng, S. A. Yang, T. Neupert, H. Lin, and M. Z. Hasan, Sci. Rep. **7**, 1688 (2017).
[30] H. Weng, C. Fang, Z. Fang, and X. Dai, Phys. Rev. B **93**, 241202(R) (2016).
[31] Z. Zhu, G. W. Winkler, Q. S. Wu, J. Li, and A. A. Soluyanov, Phys. Rev. X **6**, 031003 (2016).
[32] B. Q. Lv, Z.-L. Feng, Q.-N. Xu, X. Gao, J.-Z. Ma, L.-Y. Kong, P. Richard, Y.-B. Huang, V. N. Strocov, C. Fang, H.-M. Weng, Y.-G. Shi, T. Qian, and H. Ding, Nature (London) **546**, 627 (2017).
[33] G. Chang, S.-Y. Xu, B. J. Wieder, D. S. Sanchez, S.-M. Huang, I. Belopolski, T.-R. Chang, S. Zhang, A. Bansil, H. Lin, and M. Z. Hasan, Phys. Rev. Lett. **119**, 206401 (2017).
[34] P. Tang, Q. Zhou, and S.-C. Zhang, Phys. Rev. Lett. **119**, 206402 (2017).
[35] B. Bradlyn, J. Cano, Z. Wang, M. G. Vergniory, C. Felser, R. J. Cava, and B. A. Bernevig, Science **353**, aaf5037 (2016).
[36] J. L. Mañes, Phys. Rev. B **85**, 155118 (2012).
[37] D. Hsieh, D. Qian, L. Wray, Y. Xia, Y. S. Hor, R. J. Cava, and M. Z. Hasan, Nature (London) **452**, 970 (2008).
[38] C.-Z. Chang *et al.*, Science **340**, 167 (2013).
[39] S.-Y. Xu, I. Belopolski, N. Alidoust, M. Neupane, G. Bian, C. Zhang, R. Sankar, G. Chang, Z. Yuan, C.-C. Lee, S.-M. Huang, H. Zheng, J. Ma, D. S. Sanchez, B. Wang, A. Bansil, F. Chou, P. P. Shibayev, H. Lin, S. Jia, and M. Z. Hasan, Science **349**, 613 (2015).
[40] See Supplemental Material at http://link.aps.org/supplemental/10.1103/PhysRevLett.130.066402 for Sec. I. A., which provides a discussion of previous research on topological chiral crystals; Secs. I. B., I. C., and II. A. for material growth and characterization details, which include Refs. [41–44]; Sec. II. B. for an explanation of photoemission experiment methods, which includes Refs. [45–48]; Secs. I. D. and II. C. for sum-frequency results, which include Refs. [49–53]; and Secs. I. E. for photocurrent results, which include Refs. [54,55].
[41] Y. Liu, Z. Li, L. Guo, X. Chen, Y. Yuan, F. Liu, S. Prucnal, M. Helm, and S. Zhou, J. Magn. Magn. Mater. **408**, 73 (2016).
[42] D. Shoenberg and M. Z. Uddin, Proc. R. Soc. Lond. A **156**, 701 (1936).

[43] Y. Fuseya, M. Ogata, and H. Fukuyama, J. Phys. Soc. Jpn. **84**, 012001 (2015).
[44] T. Muro, Y. Senba, H. Ohashi, T. Ohkochi, T. Matsushita, T. Kinoshita, and S. Shin, J. Synchrotron Radiat. **28**, 1631 (2021).
[45] V. Strocov, J. Electron Spectrosc. Relat. Phenom. **130**, 65 (2003).
[46] V. N. Strocov, M. Shi, M. Kobayashi, C. Monney, X. Wang, J. Krempasky, T. Schmitt, L. Patthey, H. Berger, and P. Blaha, Phys. Rev. Lett. **109**, 086401 (2012).
[47] I. Belopolski, S.-Y. Xu, D. S. Sanchez, G. Chang, C. Guo, M. Neupane, H. Zheng, C.-C. Lee, S.-M. Huang, G. Bian, N. Alidoust, T.-R. Chang, B. K. Wang, X. Zhang, A. Bansil, H.-T. Jeng, H. Lin, S. Jia, and M. Z. Hasan, Phys. Rev. Lett. **116**, 066802 (2016).
[48] T. Morimoto and N. Nagaosa, Sci. Adv. **2**, e1501524 (2016).
[49] G. Kresse and D. Joubert, Phys. Rev. B **59**, 1758 (1999).
[50] D. E. Parker, T. Morimoto, J. Orenstein, and J. E. Moore, Phys. Rev. B **99**, 045121 (2019).
[51] Z. Ni, B. Xu, M.-Á. Sánchez-Martínez, Y. Zhang, K. Manna, C. Bernhard, J. W. F. Venderbos, F. de Juan, C. Felser, A. G. Grushin, and L. Wu, npj Quantum Mater. **5**, 96 (2020).
[52] Z. Ni, K. Wang, Y. Zhang, O. Pozo, B. Xu, X. Han, K. Manna, J. Paglione, C. Felser, A. G. Grushin, F. de Juan, E. J. Mele, and L. Wu, Nat. Commun. **12**, 154 (2021).
[53] S. D. Huber, Nat. Phys. **12**, 621 (2016).
[54] L. Lu, J. D. Joannopoulos, and M. Soljačić, Nat. Photonics **8**, 821 (2014).
[55] N. Goldman, J. C. Budich, and P. Zoller, Nat. Phys. **12**, 639 (2016).
[56] J. C. H. Spence, J. M. Zuo, M. O'Keeffe, K. Marthinsen, and R. Hoier, Acta Crystallogr. Sect. A **50**, 647 (1994).
[57] V. N. Strocov, X. Wang, M. Shi, M. Kobayashi, J. Krempasky, C. Hess, T. Schmitt, and L. Patthey, J. Synchrotron Radiat. **21**, 32 (2014).
[58] L. Wu, S. Patankar, T. Morimoto, N. L. Nair, E. Thewalt, A. Little, J. G. Analytis, J. E. Moore, and J. Orenstein, Nat. Phys. **13**, 350 (2017).
[59] G. Kresse and J. Furthmüller, Phys. Rev. B **54**, 11169 (1996).
[60] Y. Liu, X. Chen, and Y. Xu, Adv. Funct. Mater. **30**, 1904784 (2020).
[61] F. Mei, Q. Guo, Y.-F. Yu, L. Xiao, S.-L. Zhu, and S. Jia, Phys. Rev. Lett. **125**, 160503 (2020).
[62] P. Delplace, J. B. Marston, and A. Venaille, Science **358**, 1075 (2017).